Journal of Chemical Health Risks

www.jchr.org

JCHR (2025) 15(3), 01-07 | ISSN:2251-6727

Cytotoxicity, Apoptotic properties and ROS expression of biosynthesized silver nanoparticles from endophytic fungus *Lasiodiplodia pseudotheobromae* on Caco2 and HepG2 cell lines

Pooja Vidyasagar Gunagambhire[1], Kariyellappa Nagaraja Shashiraj[1] and Sreenivasa Nayaka[1,*]

[1] P.G. Department of Studies in Botany, Karnatak University, Dharwad-580003, Karnataka, India.

(Received: 16 March 2025 Revised: 20 April 2025 Accepted: 15 June 2025)

KEYWORDS

Endophytic fungus, Lasiodiplodia pseudotheobromae, Myco-fabrication, ROS expression, Biological assays

ABSTRACT:

Nanotechnology has revolutionized biomedical applications, with silver nanoparticles (AgNPs) gaining attention for their antimicrobial and anticancer properties. Traditional synthesis methods often involve toxic chemicals, prompting the need for eco-friendly alternatives. This study reports the green synthesis of AgNPs using the endophytic fungus Lasiodiplodia pseudotheobromae isolated from Gloriosa superba leaves. The biosynthesized PSEF2-AgNPs were characterized using UV-Vis spectroscopy, FTIR, SEM, TEM, XRD, zeta and DLS, revealing spherical morphology, crystalline structure, and stability with size 5–29 nm. The nanoparticles exhibited potent antimicrobial activity against pathogenic bacteria and yeasts, along with significant antioxidant properties in DPPH and H_2O_2 scavenging assays. In vitro cytotoxicity studies demonstrated dose-dependent anticancer effects against Caco2 and HepG2 cell lines, with IC_{50} values of 97.74 µg/mL and 96.54 µg/mL, respectively. Apoptotic induction was confirmed through Annexin V/PI staining, AO/EtBr fluorescence assays, and ROS generation, indicating oxidative stress-mediated cell death. These findings support the therapeutic potential of PSEF2-AgNPs as multifunctional agents. Future research should focus on in vivo validation, mechanistic studies, and scalable production to advance their clinical application.

1. Introduction

Nanotechnology, a swiftly advancing scientific field, has significantly influenced human life. Nanoparticles are atomic clusters measuring between 1 to 100 nm, characterized by unique properties such as diminutive size, chemical stability, and biological attributes (Khan et al., 2022). Nanoparticles distinctive dimensions, morphology, and composition enable them to engage with various biological entities, including bacteria, actinomycetes, fungi, plants, and animals. Various metals like magnesium, platinum, titanium, copper, gold, zinc, and silver are promising candidates for nanoparticle synthesis (Chakraborty et al., 2021). AgNPs exceptional physical, chemical, and biological properties have attracted considerable interest in recent years, and extensive research has proposed various methods for their synthesis. The widespread use of AgNPs is limited by the unsustainable characteristics of traditional physical and chemical synthesis methods, posing significant health risks due to the use of toxic substances. Consequently, there is an increasing demand for eco-friendly methods of synthesizing AgNPs (Ahmed et al., 2016). The biological means of production of AgNPs are non-toxic, effective, simple, and cost-effective. The biomedical, pharmaceutical, food, cosmetic, sewage treatment, and diagnostic industries use these methods in gene therapy, biosensors, antibacterial, antiviral, antidiabetic, anti-inflammatory, and cancer treatments (Bhattacharya and Mukherjee, 2008; Guilger-Casagrande and Lima 2019). Silver has been used for its antimicrobial and disinfectant properties since ancient times. Biogenic AgNPs are popular due to their stability, chemical and physical properties, and low toxicity (Burdușel et al., 2018).

Gloriosa superb L., prized for its striking, vividly coloured flowers, belongs to the family Colchicaceae. It is a native to tropical and southern Africa and parts of Asia and some parts of Australia and the Pacific. These are tender, tuberous-rooted deciduous

Journal of Chemical Health Risks
www.jchr.org
JCHR (2025) 15(3), 01-07 | ISSN:2251-6727

perennials. Despite their beauty, all parts of the plant, especially the tubers are highly toxic due to the presence of colchicine. The plant contains several bioactive compounds, including isoperlolyrine, colchicine, sitosterol, tropolane, and luteolin. Traditionally, *G. superba* has been widely used in folk medicine. Colchicine extracted from the plant is clinically used to treat acute gout and is also effective against infertility, intestinal worms, skin disorders and wounds. The roots and leaves have been employed a laxative, antidote for snake bites and for inducing abortion. Other medicinal applications include the treatment of chronic ulcers, cholera, arthritis, kidney disorders, colic, and typhus. The broad pharmacological profile of *G. superba* underscores its significance in traditional medicine (Kavithamani et al., 2013; Joshi et al., 2024). Hence the plant stands as an excellent candidate for nanoparticle synthesis due to its rich phytochemical profile.

The synthesis of AgNPs through fungal endophytes represents an innovative method for developing a nontoxic, permeable, and cost effective nano drug. This approach provides a novel strategy for the early detection, diagnosis, and treatment of severe diseases, including cancer (Barik et al., 2020). Endophytic fungi are microorganisms that live inside plant tissues forming a symbiotic relationship with the host plant (Juan et al., 2022). A number of endophytic fungi were isolated from different parts of *G. superba* such as *Botryodiplodia theobromae*, *Colletotrichum gleosporoides*, *Fusarium oxysporum*, *Talaromyces pinophilus*, *Curvularia lunata*, *Trichoderma asperellum*, *Bipolaris cynodontis*, etc. (Shobha et al., 2019). The synthesis of fungus-mediated AgNPs has been widely reported. *Penicillium* sp. isolated from *Glycosmis mauritiana* efficiently produced AgNPs exhibiting strong antioxidant, antimicrobial, anti-inflammatory, and tyrosinase inhibitory activities. Similarly, *Talaromyces purpureogenus* isolated from *Pinus* sp. generated AgNPs with notable antibacterial and antioxidant properties. *Taxus baccata* is also recognized as a rich host of diverse fungal species. AgNPs were synthesized from *Nemania* sp. isolated from *Taxus baccata*, displaying significant antibacterial effects against pathogenic bacteria. A study employed *Talaromyces purpureogenus* isolated from *Taxus baccata* for AgNP synthesis. The nanoparticles showed effective antibacterial and antioxidant properties (Sharma et al., 2022).

Human colorectal adenocarcinoma cell line (Caco2) was obtained from colon and rectal cancer cells. Colon cancer originates in the epithelial cells of the large intestine and is one of the most common cancers globally ranking just after lung and prostate cancers in men and breast cancer in women. It is often linked to genetic mutations, diet, and lifestyle factors. Despite advancements in treatment, stage-IV metastatic colon cancer remains largely incurable. This underscores the urgent need for new therapeutic targets (Sergei et al., 2021).

Hepatocellular carcinoma (HCC) is the most common form of primary liver cancer, accounting for over 80% of cases globally. HepG2 is a HCC cell line derived from a liver tumor. Its development is a complex, multistep process involving liver injury, chronic inflammation, fibrosis, cirrhosis, and ultimately malignant transformation. Molecular mechanisms contribute to HCC pathogenesis include cell cycle deregulation, altered DNA methylation, chromosomal instability, immune modulation, and mi-RNA dysregulation. The disease is frequently linked to chronic liver diseases such as hepatitis B and C infections, cirrhosis, and metabolic disorders. Due to its aggressive progression and typically late diagnosis, HCC carries a high mortality rate, emphasizing the urgent need for innovative treatment strategies (Saranya et al., 2021). Conventional cancer treatments, including radiotherapy and chemotherapy, have been shown to produce a variety of side effects, some of which can adversely affect healthy cells. Consequently, AgNPs produced from diverse biological extracts have been recognized as potential anticancer agents for managing multiple cancer types (Math et al., 2023).

The novelty of this work lies in the eco-friendly biosynthesis AgNPs using the endophytic fungus *Lasiodiplodia pseudotheobromae* isolated from *G. superba* L. leaves, that has not been previously reported. The synthesized AgNPs were characterized with different techniques and their antimicrobial, antioxidant, and anticancer properties including induction of apoptosis and reactive oxygen species (ROS) generation were evaluated. The work highlights the potential of fungal endophytes as a novel source for

Journal of Chemical Health Risks
www.jchr.org
JCHR (2025) 15(3), 01-07 | ISSN:2251-6727

biomedical applications and offers a promising alternative for cancer therapy and pathogen control. This research contributes to the growing field of green nanotechnology by providing a cost-effective, environmentally friendly, and scalable method for AgNP production with broad therapeutic applications.

2. Materials and Methods

2.1. Collection and isolation of endophytic fungus from *Gloriosa superba* L.

Healthy and symptomless *Gloriosa superba* L. leaves were collected from the campus of the Department of Botany, Gulbarga University, and taxonomically identified. A herbarium specimen (No. KU/BOT-GSM/2022-23/SN-PVG-5/21) was submitted to the Department of Botany, Karnatak University, Dharwad, Karnataka, India. The healthy leaf samples were put into sterile zipper bags and transferred to the laboratory. The leaf samples were washed with double distilled water and dried with sterile filter paper; then cut into small pieces. Small pieces of leaves were sterilized with 75% ethanol for 2 min, 2.5% sodium hypochlorite for 4 min, and a final rinsing three times in sterile distilled water. The sterilized leaf segments were placed on potato dextrose agar (PDA) plates and incubated at 25 ±2 °C for 5 to 7 days until the fungal isolate grows surrounding leaf section. Emerging fungal isolate was sub-cultured on PDA and stored at -20 °C for further use.

2.2. Morphological and molecular characterization of isolate PSEF2

The isolated endophytic fungus PSEF2 was cultured on PDA medium at 25 ± 2 °C for 5-7 days. Morphological features such as colony shape, pigmentation, mycelia, and conidia structure were examined under a compound microscope and further analyzed using scanning electron microscopy (SEM). For molecular identification, genomic DNA was extracted, and the ITS region of rDNA was amplified using universal primers ITS_5 and ITS_4. Sequencing was performed using the ABI BigDye® Terminator v3.1 kit on a SeqStudio DNA sequencer. The resulting sequence was compared against fungal ITS databases and submitted to NCBI, where it was assigned an accession number. A phylogenetic tree was constructed using MEGA 7.0 software through neighbor-joining analysis with related sequences from the NCBI database.

2.3. Preparation of fungal broth and synthesis of silver nanoparticles

PSEF-2AgNPs were synthesized using the fungal strain *L. pseudotheobromae* PSEF2, following a protocol based on Wang et al. (2021) with minor modification. The fungus was cultured in PDB with the pH adjusted to 7.0 and inoculated with 1×10^6 spores in 250 mL flasks. These flasks were incubated at 25 °C in an orbital shaker at 150 rpm for 7 days. After incubation, the fungal biomass was removed using Whatman filter paper, and the cell-free supernatant was collected.

To synthesize PSEF-2AgNPs, silver nitrate solution was mixed with the fungal supernatant in a 1:3 ratio (supernatant:$AgNO_3$) in a 200 mL flask. This mixture was incubated in the dark for 3h to allow nanoparticle formation. The resulting PSEF-2AgNPs were separated by centrifugation at 10,000 rpm for 1h, washed thoroughly with double-distilled water to remove any residual impurities, and dried in a hot air oven at 40 °C for further characterization.

2.4. Characterization of PSEF-2AgNPs:

The size, shape, structure, and surface characteristics of the synthesized PSEF2-AgNPs were confirmed using various analytical techniques. UV-Vis spectroscopy (METASH UV-9600A, Shanghai, China) was employed to detect the characteristic surface plasmon resonance of the AgNPs within the 300–700 nm range, confirming nanoparticle formation (Seetharaman et al., 2021). Fourier Transform Infrared (FTIR) Spectroscopy (NICOLET 6700 FTIR Spectrophotometer, Waltham, MA, USA) identified functional groups in both the PSEF2 extract and the PSEF2-AgNPs at 400-4000 cm^{-1} range and a resolution of 4 cm^{-1}. This analysis provided insights into the biomolecules involved in capping and stabilization (El-Zawawy et al., 2023). Energy Dispersive Spectroscopy (EDS) (JEOL JSM-IT500LA, USA) was used to determine the elemental composition of the nanoparticles, confirming the presence of silver. Scanning Electron Microscopy (SEM) offered details

Journal of Chemical Health Risks
www.jchr.org
JCHR (2025) 15(3), 01-07 | ISSN:2251-6727

about the surface morphology and texture of the nanoparticles. For high-resolution imaging, Transmission Electron Microscopy (HRTEM) (FEI TECNAI G2 F30, Beijing, China) was used to analyze the size and morphology of the PSEF2-AgNPs at 6000x to 8000x magnification. The images were processed using J1.45s software (Ali et al., 2024). X-ray Diffraction (XRD) (Rigaku Miniflex 600, Smart-Lab SE) was applied to assess the crystalline nature, phase purity, and average crystallite size of the nanoparticles. XRD was analysed with a CuKα filter (λ = 0.15418 nm) and at 5°–80° range the spectrum was recorded and confirmed with JCPDS card No. 04-0783 (Tyagi et al., 2019). Surface charge and colloidal stability were assessed using zeta potential analyser (HORIBA SZ-100 nanoparticle analyzer, Kyoto, Japan). In addition, Dynamic Light Scattering (DLS) measurements were performed to determine the hydrodynamic diameter and dispersion quality of the PSEF2-AgNPs in suspension. Together, these methods provided comprehensive characterization of the PSEF2-AgNPs, confirming their successful synthesis and stability (Liaqat et al., 2022; Rudrappa et al., 2023).

2.5. Evaluation of synthesized AgNPs for antimicrobial activity

The antimicrobial activity of biosynthesized PSEF2-AgNPs was evaluated against *Escherichia coli* (MTCC 40), *Pseudomonas aeruginosa* (MTCC 9027), *Bacillus subtilis* (MTCC 6633), *Staphylococcus aureus* (MTCC 6908), *Candida albicans* (MTCC 227), and *Candida glabrata* (MTCC 3019) using the agar well diffusion method, as described by Enerelt et al. (2021). PSEF2-AgNPs suspension in DMSO (1 mg/mL) was prepared. Bacterial and yeast cultures, standardized to 0.5 McFarland, were uniformly swabbed onto nutrient agar plates using sterile cotton buds. Wells of 6 mm diameter were made using a sterile cork borer, into which varying volumes (25, 50, 75, and 100 µL) of the PSEF2-AgNPs suspension were added. Streptomycin (25 µL) was used as the positive control for bacterial strains, while amphotericin B was used for fungal strains. Sterile distilled water served as the negative control. All plates were incubated at 37 °C for 24 h. Post-incubation, the diameter of the inhibition zones was measured and compared to the controls to assess antimicrobial efficacy (Vasudeva et al., 2016).

2.6. Antioxidant activity of silver nanoparticles

2.6.1. Quantification of DPPH activity

The free radical scavenging activity of biosynthesized PSEF2-AgNPs was evaluated using the 2,2-diphenyl-1-picrylhydrazyl (DPPH) assay, following the method described by Hikmet and Hussein, (2021). Ascorbic acid was used as the standard reference antioxidant. Various concentrations of PSEF2-AgNPs and standard (50, 100, 150, 200 and 250 µg/mL) were mixed with 3 mL of DPPH solution and incubated in the dark for 30 min to prevent photo-degradation. Absolute methanol served as the blank, while DPPH solution without any test sample was used as the control. Absorbance was recorded at 517 nm using a UV–Visible spectrophotometer. The radical scavenging activity was calculated, and results were expressed as IC_{50} value (µg/mL).

$$\% \text{ of radical scavenging activity} = \frac{\text{Absorbance of control} - \text{Absorbance of sample}}{\text{Absorbance of control}} \times 100$$

2.6.2. Hydrogen peroxide (H_2O_2) scavenging activity

A 40 mM H_2O_2 solution was prepared in phosphate buffer (pH 7.4). Various concentrations (50, 100, 150, 200 and 250 µg/mL) of the PSEF2-AgNPs or ascorbic acid (standard) were mixed with 0.1 mL of the H_2O_2 solution. After 10 min of incubation, the absorbance was measured at 230 nm against a blank containing only phosphate buffer (without H_2O_2). The H_2O_2 scavenging activity was calculated using a standard formula (Alsareii et al., 2022).

$$\% \text{ of } H_2O_2 \text{ scavenging activity} = \frac{\text{Absorbance of control} - \text{Absorbance of sample}}{\text{Absorbance of control}} \times 100$$

2.7. Assessment of the cytotoxicity of PSEF2-AgNPs

The MTT assay was used to determine the cytotoxicity of synthesized PSEF2-AgNPs against Caco2 and HepG2 cell lines. The Caco2 and HepG2 cells were cultivated in DMEM supplemented with 10% FBS for 24 h at 37 °C, with 5% CO2 and 95% humidity for cell proliferation. Following incubation, 200 µL of medium containing ~20,000 cells/well was dispensed in a 96-well plate. Then, different concentrations of PSEF2-AgNPs (12.5, 25, 50, 100 and 200 µg/mL) were added

Journal of Chemical Health Risks
www.jchr.org
JCHR (2025) 15(3), 01-07 | ISSN:2251-6727

to culture media and incubated at 37 °C for 24 h. The doxorubicin (4 µM/mL) was positive control and the medium containing cells with no treatment was negative control. The 200 µL of MTT solution was prepared, added to each well, and incubated at 37 °C for 4 h. The following incubation formazan crystals were dissolved in 100 µL of DMSO. A microplate reader, (ELX-800, BioTek, Winooski, VT, USA) set to 570 nm was used to determine the cell viability. Y = Mx + c is the equation used to calculate the IC_{50} value, which was determined using the procedure outlined by Chakraborty et al., (2021).

2.8. FITC Annexin-V/ propidium iodide (PI) apoptosis detection assay

This assay was carried out for the quantification of early and late apoptotic cells. The apoptotic activity of PSEF2-AgNPs was evaluated in Caco2 and HepG2 cancer cell lines using FITC Annexin-V and PI staining, following the method described by Rudrappa et al. (2023). Cells were treated with the IC_{50} concentration of PSEF2-AgNPs in a 96-well plate. After treatment, cells were harvested using 200 µL of trypsin-EDTA, washed with PBS at 37 °C for 3-4 min, and centrifuged at 300 rpm for 5 min. Subsequently, 5 µL each of Annexin-V and PI were added, and the cells were incubated in the dark for 15 min. The stained cells were then washed twice with PBS and resuspended in 400 µL of 1X binding buffer. Doxorubicin was used as the positive control, while untreated cells served as the negative control. Fluorescence was analyzed using a BD FACS Calibur flow cytometer, and data were processed using BD Cell Quest Pro version 6.0.

2.9. Acridine orange (AO), Ethidium bromide (EtBr) staining

Condensed apoptotic and necrotic nuclei were observed in Caco2 and HepG2 cells treated with the IC_{50} concentration of synthesized PSEF-2 AgNPs. After 24 h of exposure, the cells were washed with PBS and stained with AO and EtBr, using 1 µL of each dye. Fluorescence microscopy was performed using a compound microscope equipped with a 488 nm excitation and 525 nm emission filter. Cell viability was assessed based on fluorescence patterns: green nuclei indicated live cells, green chromatin condensation suggested apoptosis, and intact orange nuclei signified necrosis. This staining method provided clear differentiation between viable, apoptotic, and necrotic cells to confirm the cytotoxic effect of PSEF-2 AgNPs (Ahmed et al., 2016; Liaqat et al., 2022).

2.10. Reactive oxygen species (ROS) assay

For the ROS assay, cancer cells (10,000 cells/200 µL) were seeded in a 96-well plate and treated with PSEF-2 AgNPs at their IC_{50} concentration. The cells were incubated at 37 °C with 5% CO_2 for 24 h. In post-incubation, cells were washed with 1X PBS and exposed to 100 µM H_2O_2 as a ROS inducer and incubated for 30 min. After treatment, the cells were harvested, washed twice with PBS, and stained with 5 µM 2′,7′-dichlorodihydrofluorescein diacetate (H_2DCFDA), a ROS-sensitive fluorescent probe, followed by 40 min incubation in the dark at 37 °C. Further, the cells were rinsed with PBS and fluorescence imaging was performed using a ZEISS LSM 80 confocal microscope with excitation at 341 nm and emission at 452 nm. ZEN Blue software was used for image analysis, while ImageJ software was employed to quantify dichlorofluorescein (DCF) intensity (Das et al., 2017).

2.11. Statistical analysis

The experiments were administered in triplicate (n = 3), and the data were furnished as the mean value along with the standard deviation (±SD) along with ANOVA. The analyses were performed using Graph Pad prism 9.0, and OriginPro 2022b softwares.

3. Results and Discussion

3.1. Morphology and Molecular identification of endophytic fungi

Endophytes are microorganisms that inhabit various plant parts and cause no damage to the host plants. The present study investigates synthesis of AgNPs from an endophytic fungus *L. pseudotheobromae* from *G. superb* L. During morphological characterizations, the fungal colonies initially appeared white with sparse, fluffy aerial mycelia, turned pale gray with dark pigmentation after (Figure 1A). Pycnidia were solitary, globose, and dark

Journal of Chemical Health Risks
www.jchr.org
JCHR (2025) 15(3), 01-07 | ISSN:2251-6727

brown to black. Mycelia were hyaline, aseptate, cylindrical, sometimes branched. Conidia were oval shaped, thick-walled with rounded ends, while mature conidia were dark brown (Figure 1B and 1C). In a similar report Chen et al, (2021) isolated a fungus and it was identified as *L. pseudotheobromae*. Similarly de Silva et al, (2019) isolated *L. pseudotheobromae* from the twig and leaf of *M. candolii* as an endophyte.

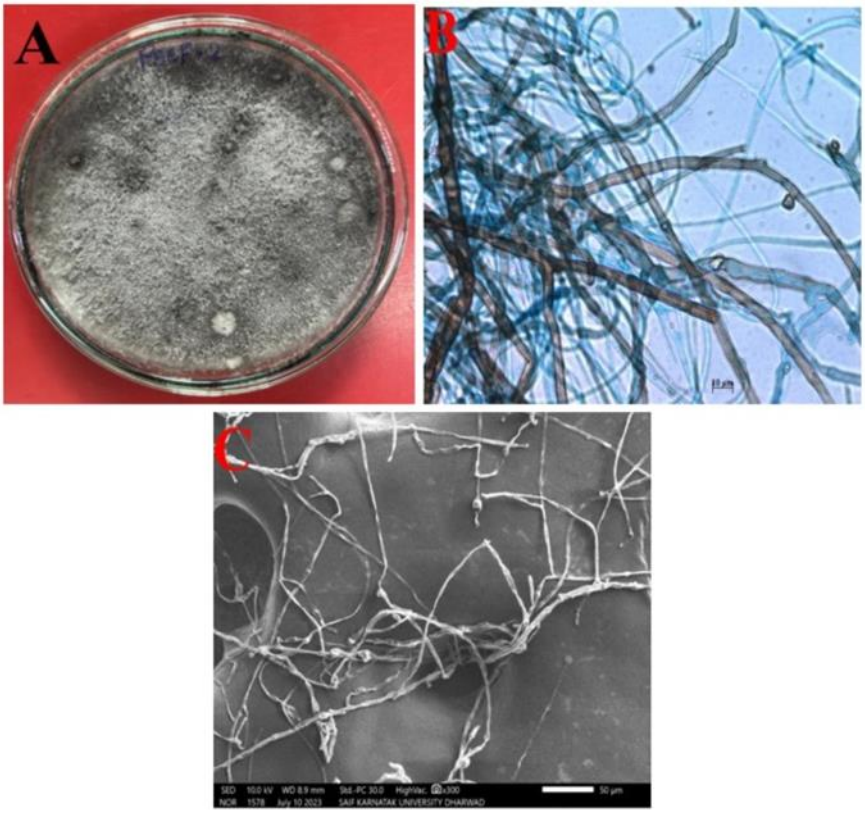

Figure 1. Morphological characterization of *L. pseudotheobromae* PSEF2: (A) Blackish colored aerial mycelia, (B) Optical microscope image of fungus Hyphae, and (C) Image of SEM showing fungal mycelia.

The endophytic fungus was identified through genotypic characterization, revealing a 480 base pair sequence in the ITS region. This sequence was submitted to the NCBI GenBank database under the accession number PQ569346. Morphological and molecular analyses confirmed the isolate as *Lesiodiplodia pseudotheobromae* PSEF2. Phylogenetic analysis further supported this identification, showing that PSEF2 clustered closely with known *L. pseudotheobromae* species, confirming its taxonomic placement (Figure 2). This study marks the first report of eco-friendly synthesis of AgNPs using the culture supernatant of *L. pseudotheobromae* PSEF2. The ITS regions are non-coding segments within rRNA genes, flanked by conserved coding regions. Due to high variability and low selective constraints in ITS regions in fungi, these regions (typically 500-750 bp) are widely used as molecular markers for fungal diversity studies and phylogenetic analysis (Huzefa et al., 2017). In a similar study Toppo et al, (2024) isolated 5 endophytic fungi from *Anisomeles indica*. The ITS regions of these endophytes were sequenced and identified as *Colletotrichum cobbittiense*, *Colletotrichum yulongense*, *Colletotrichum cobbittiense*, *Colletotrichum alienum*, and *Fusarium equiseti*.

Journal of Chemical Health Risks
www.jchr.org
JCHR (2025) 15(3), 01-07 | ISSN:2251-6727

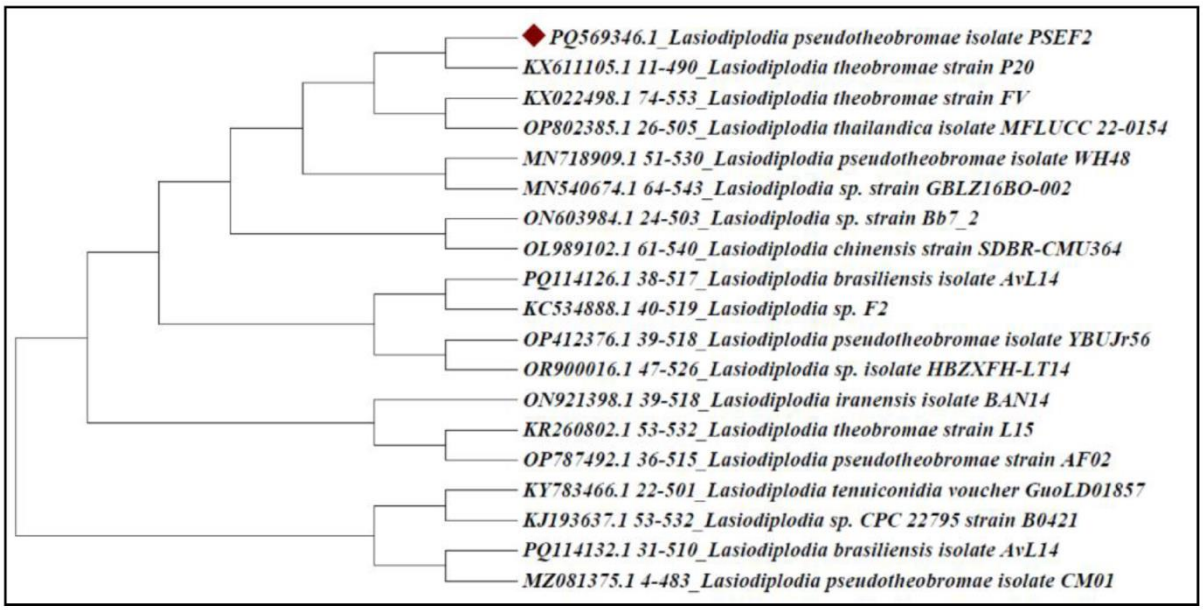

Figure 2. Phylogenetic tree of *Lasiodiplodia pseudotheobromae* PSEF2 based on ITS nucleotide sequence analysis, showing evolutionary relationships with closely related fungal species.

3.2. Synthesis of silver nanoparticles

The fungal extract reacted with silver nitrate and caused the transition of solution from pale yellow to dark brown within 3 h due to surface plasmon resonance of PSEF2-AgNPs. This colour change confirmed the biosynthesis of PSEF2-AgNPs (Figure 3A). This colour shift signified the reduction of silver ions into nanoparticles and demonstrated the extract's ability to facilitate AgNP formation. Fungal cell-free extracts offer an eco-friendly and cost-effective approach for synthesis of nanoparticle, making them a promising alternative to conventional methods. The biosynthesis of PSEF2-AgNPs using fungal supernatant occurs primarily through extracellular reduction. Bioactive metabolites and enzymes secreted by the fungus facilitate the reduction of silver ions (Ag^{+}) to metallic silver (Ag^{0}). When fungal supernatant is mixed with silver nitrate reduction of Ag^{+} ions takes place. The fungal supernatant contains redox-active enzymes such as NADH-dependent reductases, peroxidases, periplasmic nitrate reductases etc. as well as secondary metabolites (e.g., phenolic compounds, quinones, and organic acids). These biomolecules donate electrons to Ag^{+} ions, reducing them to Ag^{0} atoms, which nucleate to form AgNPs (Safi and Jam, 2021). Certain amino acids including aspartic acid, arginine, glutamic acid, cysteine, methionine and lysine play a role in reducing Ag^{+} to Ag^{0}. This process generates hydroxyl ions, which then react with reducing agents. Additionally, it was demonstrated that peptides with disulfide bonds can also facilitate the reduction of Ag^{+} to Ag^{0} (Ekaterina, 2020). Birla et al., (2013) indicated that the excitation of surface plasmon after treatment with silver nitrate results in the fungal cell filtrate changing from pale yellow to dark brown. The synthesis of silver nanoparticles exhibits significant absorption in the visible spectrum due to local surface plasmon resonance. Studies on *Aspergillus sydowii* showed the colour change from yellow to brown when cell filtrate was mixed with silver nitrate solution (Wang et al., 2021). Similarly, the extracellular synthesis of AgNPs was observed in *Macrophomina phaseolina*, where redox proteins on the cell wall surface facilitated the reduction of Ag^{+} ions (Spagnoletti et al., 2019).

3.3. Characterizations of PSEF2-AgNPs

3.3.1. UV-Visible Spectroscopy

PSEF2-AgNPs synthesized from endopyhtic fungus were confirmed via UV-visible spectroscopy at 300-700 nm. An absorption peak at 418 nm supports the formation of PSEF2-AgNP synthesis (Figure 3B). Hu et al., (2019) reported that the highest adsorption rate from

Journal of Chemical Health Risks
www.jchr.org
JCHR (2025) 15(3), 01-07 | ISSN:2251-6727

390 nm to 420 nm for the nanoparticles supports the formation of AgNPs, thereby confirming results. The presence of this sharp peak confirms the successful synthesis of PSEF2-AgNP. The position and intensity of the peak suggest that the nanoparticles are well-dispersed, spherical, and relatively small in size. Additionally, the absence of secondary peaks indicates the purity and polydispersity of the PSEF2-AgNP. In a similar study Wang et al., (2021), reported a strong absorbance peak at 420 nm, which indicated a successful biosynthesis of AgNPs.

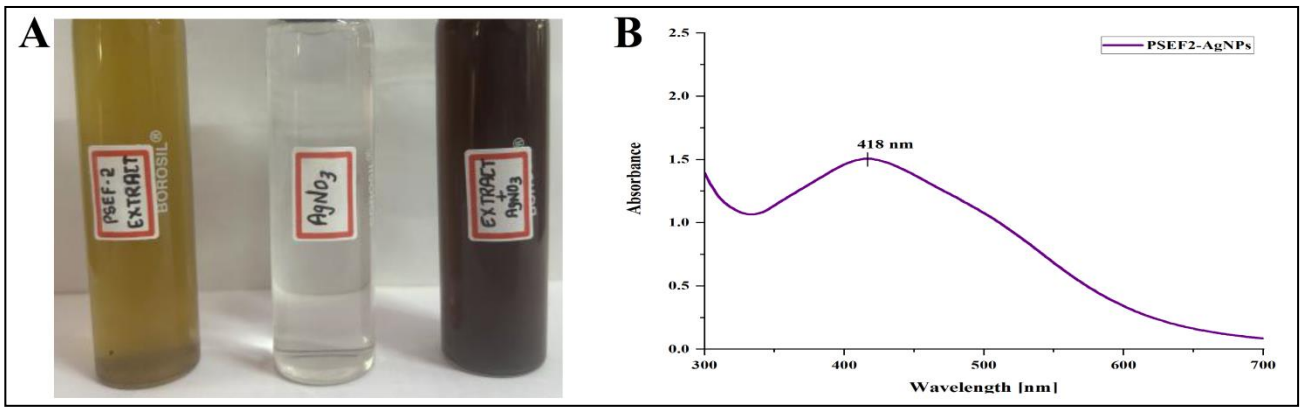

Figure 3. Characterization of PSEF2-AgNPs: (A) Color change from pale yellow to brown indicating the successful biosynthesis of PSEF2-AgNPs by the extract of *L. pseudotheobromae* PSEF2, confirming the reduction of Ag^{+} to Ag^{0} and (B) UV–Visible absorption spectrum confirming the formation of PSEF2-AgNPs with a characteristic peak at 418 nm.

3.3.2. FTIR analysis

FTIR spectroscopy provides crucial insight into the surface chemistry and stabiliza-tion mechanisms of biosynthesized nanoparticles. In this study, the FTIR spectra of both the *L. pseudotheobromae* PSEF2 extract and the PSEF2-AgNPs revealed significant differences, indicating the involvement of various biomolecules in nanoparticle formation and stabilization. PSEF2 extract displayed 11 strong bands and 16 bands corresponded to PSEF2-AgNPs (Figure 4A and 4B). The functional groups of PSEF2 extract displayed the peak at 3404 cm^{-1} showing a strong, broad band indicating the presence of O-H stretching alcohol, 2924 cm^{-1} depicts C-H stretching alkene, strong peak at 1731 cm^{-1} and 1641 cm^{-1} band shows C=O stretching aldehyde and C=N stretching secondary amide, 1377 cm^{-1} confirms O-H binding alcohol, Vinyl ether shows at 1225 cm^{-1} shows the strong peak nature, 1021 cm^{-1} depicts C-N stretching amine, 914 cm^{-1} interprets the C-H binding vibrations in alkene, 838 cm^{-1} band shows C=C binding of halo compound, 774 cm^{-1} confirms C-H binding 1,2,3-trisubstituted bond, and C-Br stretching of halo compound shows at 620 cm^{-1} shows the strong peak nature. The absorption 16 bands of synthesized PSEF2-AgNPs with different functional groups, the peak at 3419 cm^{-1} shows O-H stretching alcohol, 1635 cm^{-1} interprets C=C stretching alkene, 1559 cm^{-1} corresponds to N-O stretching vibration, 1477 cm^{-1} confirms C-H binding alkane, 1383 cm^{-1} shows a medium band indicating the presence of C-H binding aldehyde, 1312 cm^{-1} depicts O-H bending phenol, 1247 cm^{-1} interprets the C-O stretching alkyl aryl ether, 1181 cm^{-1} peak indicate the C-O stretching ester, 1080 cm^{-1} confirms C-O stretching primary alcohol, plane bending vibrations in alkene shows at 913 cm^{-1}, 874 cm^{-1} depicts C-H bending 1,3-disubstituted strong peak, 835 cm^{-1} interprets the C=C bending vibrations in alkene, 789 cm^{-1} band shows the C-H bending of 1,2,3-trisubstituted compound, the strong band at 678, 617 and 521 cm^{-1} confirm C-Br stretching halo compounds. Similarly, the biosynthesis of metal nanoparticles by the fungus *Botryodiplodia theobromae* exhibited the presence of free OH and NH groups, aromatic CH stretch, C-C stretch, molecular unsaturation, and C-Cl stretch (Janakiraman et al., 2019). The shift and alteration of these absorption bands confirm the participation of

Journal of Chemical Health Risks
www.jchr.org
JCHR (2025) 15(3), 01-07 | ISSN:2251-6727

proteins, phenolic compounds, and other secondary metabolites in reducing Ag^{+} ions to Ag^{0} and in capping the nanoparticles. The presence of O-H, C=O, and N-H groups suggests hydrogen bonding and electrostatic interactions that likely contribute to the stabilization of the AgNPs, preventing agglomeration (Velgosova et al., 2024). Amino acid residues and peptides in proteins exhibit a significant capacity for metal binding. Consequently, proteins are likely to form a coating around metal nanoparticles, specifically capping AgNPs to inhibit particle agglomeration and enhance stability in the medium (Sandhu et al., 2017). Furthermore, the observation of C-Br and halo compound vibrations indicates potential halogen-containing biomolecules acting as capping agents.

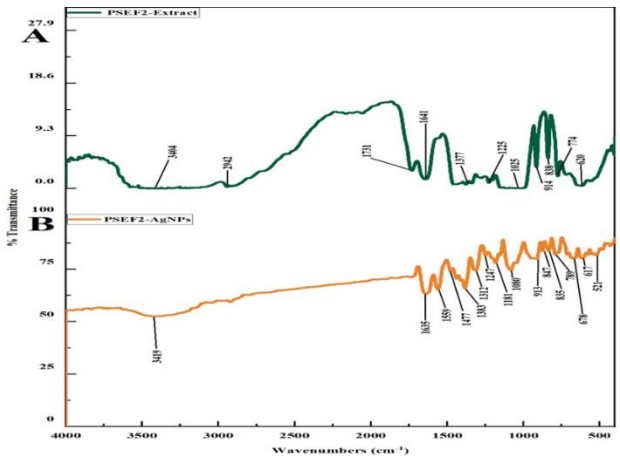

Figure 4. FTIR spectra of (A) PSEFE 2 extract and (B) PSEF2-AgNPs indicating the presence of several biological functional groups.

3.3.3. EDS analysis

The EDS spectrum confirmed the presence of silver, with a prominent peak at 3.0 keV (Figure 5), verifying the successful synthesis of PSEF2-AgNPs. Elemental analysis revealed 58.56% silver, along with carbon (10.41%) and oxygen (31.03%). The strong absorption peak at 3 keV is characteristic of pure AgNPs. This strong silver signal is indicative of the high purity and crystalline nature of the PSEF2-AgNPs. Similar reports were made by Seetharaman et al., (2018), which clearly distinguished AgNPs using the endophytic fungus *Phomopsis liquidambaris*. The synthesis of elemental silver was confirmed through EDS analysis at the binding energy of 3 keV. Similarly, the EDS study showed that silver (Ag) had the most significant signal, while chlorine, oxygen, phosphorus, sodium, and calcium had the weakest signals (Jerónimo et al., 2021).

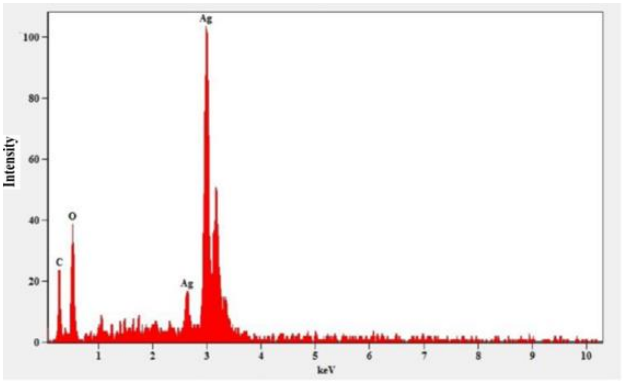

Figure 5. EDS spectrum confirming the elemental composition of the synthesized PSEF2-AgNPs with a strong silver peak at 3 keV.

3.3.4. TEM analysis

The morphology and size distribution characteristics of the biosynthesized PSEF2-AgNPs were confirmed through TEM examination, emphasizing particle size. The size of the PSEF2-AgNPs was approximately 5-29 nm. The data indicate that most biosynthesized PSEF2-AgNPs were polydisperse, spherical, and displayed minimal aggregation. The average size of the nanoparticles was determined to be 29.53 nm (Figure 6). The minimal aggregation observed suggests that the nanoparticles were well-stabilized, likely due to the capping action of biomolecules secreted by the fungal extract during the synthesis process. Similar observations were reported when synthesizing AgNPs by using *A. niger*, the same sort of nanoparticles with various shapes and sizes were found in standard biological systems with average size of 30.31 nm (Pasha et al., 2022). In another study, TEM revealed AgNPs morphology and particle size distribution in another study. The reaction mixture contained spherical AgNPs, as confirmed by TEM. The nanoparticles synthesized by *A. tamarii*, *A. niger*, and *P. ochrochloron* were 3.5 nm, 8.7 nm and 7.7 nm, respectively in size (Devi and Joshi, 2015).

Journal of Chemical Health Risks
www.jchr.org
JCHR (2025) 15(3), 01-07 | ISSN:2251-6727

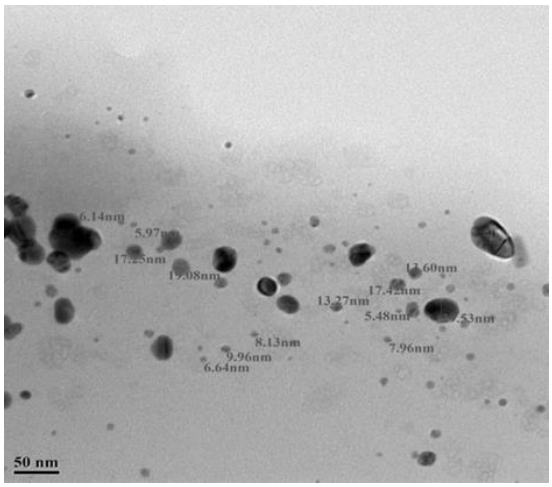

Figure 6. TEM image showing the size and morphology of biosynthesized PSEF2-AgNPs. The nanoparticles appear predominantly spherical, polydisperse, and range in size from 5–29 nm with minimal aggregation.

3.3.5. XRD analysis

The crystalline structure of the synthesized PSEF2-AgNPs was validated through powder XRD analysis. The X-ray diffraction peaks observed at approximately 38.17°, 46.26°, 64.51°, and 76.67° for 2θ values confirm the crystal planes of (111), (200), (220), and (311), which correspond to the face centred cubic (fcc) crystal structure of AgNPs as per JCPDS: 04-0783 (Figure 7). The sharp and well-defined peaks indicate high purity and crystallinity, with the absence of amorphous or impurity-related phases. The dominance of the (111) plane suggests preferential growth along this orientation due to its lower surface energy, a common feature in biologically synthesized AgNPs (Saba et al., 2025). The observed peak broadening in the XRD spectrum is attributed to the nanoscale size of the particles (5-29 nm, as confirmed by TEM), consistent with the Scherrer effect, where smaller crystallites result in broader diffraction peaks (Ungár et al., 2004). Sharma et al. (2022) reported that the endophytic fungus *Talaromyces purpureogenus*, isolated from *Taxus baccata* L., effectively synthesized AgNPs. These AgNPs were spherical, crystalline with fcc structure, and ranged in size from 30 to 60 nm.

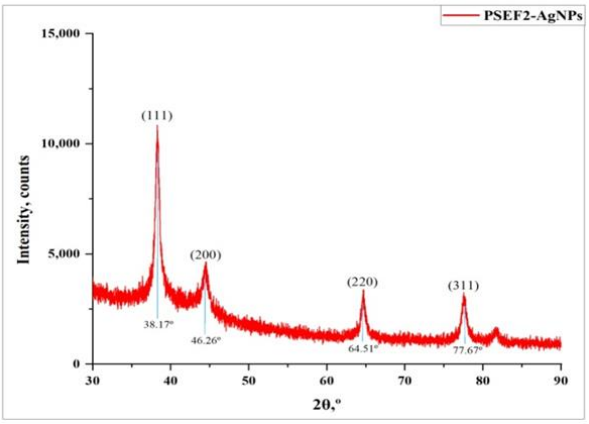

Figure 7. XRD pattern of PSEF2-AgNPs showing characteristic peaks corresponding to the crystal planes of face-centered cubic nanoparticles.

3.3.6. DLS and Zeta potential analysis

The DLS data PSEF2-AgNPs showed that the Z-average was 104.9 nm with a PdI value of 1.624 (Figure 8A). The acquired peak suggested that the quality of the produced PSEF2-AgNPs was satisfactory. The size of nanoparticles differed between TEM and DLS. TEM measures the core size of individual particles in a dry state excluding biomolecular capping agents, whereas DLS measures the hydrodynamic diameter of particles in a liquid suspension, which includes the core size, capping agents, and the hydration layer around the nanoparticles. These result in a larger apparent size compared to TEM (Xiaoyu and Gregory, 2018; Elvira et al., 2022). The surface charge of the nanomaterials acts as a determining factor in the stability and cellular responses. An aqueous solution of Ag exhibits uniform dispersion with a high level of solubility, and no agglomerates were observed until one hour. The Zeta potential value of the bioactive PSEF2-AgNPs in aqueous solution was observed to be -36.1 mV (Figure 8B). In a similar study AgNPs synthesized using the supernatant of *Trichoderma harzianum* had an average diameter of 9.6 ± 4.6 nm and ranging from 1 to 33 nm. These particles exhibited a hydrodynamic diameter of 22 nm and a zeta potential of -18.5 mV. AgNPs synthesized using the *Ganoderma sessile* showed an average size of 5.4 ± 3.0 nm and a size range of 1 to 50 nm. Their hydrodynamic diameter measured 24 nm, and the zeta potential was -23.3 mV (Elvira et al., 2022). The findings of this study are consistent with the earlier report by Iuliana et al., (2024), where the

Journal of Chemical Health Risks
www.jchr.org
JCHR (2025) 15(3), 01-07 | ISSN:2251-6727

average particle size measured by DLS was significantly higher than that observed through TEM analysis. AgNPs were synthesized using fungi like *Penicillium chrysogenum*, *Cladosporium cladosporoides* and *Purpureocillium lilacinum*. The TEM analysis revealed average particle size of 20 nm for all however the DLS analysis showed hydrodynamic diameter of 124.4 nm (*P. chrysogenum*), 165.6nm (*C. cladosporoides*), 166.7 nm (*P. lilacinum*).

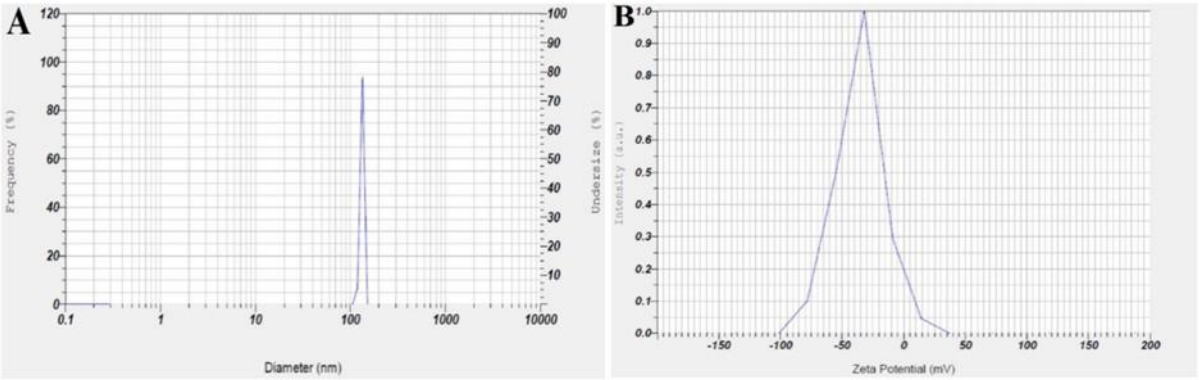

Figure 8. Characterization of PSEF2-AgNPs: (A) DLS analysis showing particle 104.9 nm (B) Zeta potential measurement (-36.1 mV) indicating their stability.

3.4. Antimicrobial activity

The antimicrobial activity of the synthesized PSEF2-AgNPs was evaluated against several human pathogens, including *S. aureus*, *E. coli*, *B. subtilis*, *P. aeruginosa*, *C. glabrata*, and *C. albicans*, using agar well diffusion method (Figure 9). The results demonstrated significant growth inhibition of the tested pathogens, even at minimal concentrations of AgNPs. The highest zone of inhibition was observed for *B. subtilis* (17.31 ± 0.18 mm), followed by *E. coli* (16.56 ± 0.36 mm), *P. aeruginosa* (16.44 ± 0.11 mm), *C. glabrata* (15.33 ± 0.10 mm), *S. aureus* (12.30 ± 0.26 mm), and *C. albicans* (12.29 ± 0.04 mm). The antimicrobial efficacy of PSEF2-AgNPs is attributed to the synergistic interaction between silver ions and bioactive molecules released from the fungal extract, which disrupt microbial cell structures and functions (Clarance et al., 2020). Similar results were reported by Singh et al., (2014), who found that AgNPs synthesized from smaller sized NPs showed increased sensitivity to *B. subtilis*, *P. aeruginosa*, *E. coli*, and *K. pneumoniae*. The results suggest that the given drug size may influence the effectiveness of AgNPs against bacteria resistant to many drugs. AgNPs exhibit potent antibacterial activity through multiple mechanisms. Silver, being positively charged readily interacts with negatively charged biomolecules such as phosphorous and sulfur, which are key components of bacterial cell membranes, DNA and proteins. Upon contact, AgNPs damage the cell wall and membrane, inducing structural deformities that compromise bacterial integrity. Studies have demonstrated the affect of AgNPs against both Gram-positive and Gram-negative pathogens, due to their ability to release Ag^+ ions continuously. These ions adhere to the cell wall and cytoplasmic membrane via electrostatic attraction and increase membrane permeability and ultimately cause cell lysis. Once internalized, Ag^+ ions disrupt cellular functions by inactivating respiratory enzymes, leading to the generation of ROS that impair ATP production. ROS further contribute to DNA damage by interacting with sulfur and phosphate groups, stop replication and bacterial proliferation. Ag^+ ions interfere with ribosomal activity, inhibit protein synthesis and denature essential cytoplasmic components. Collectively, these mechanisms membrane disruption, enzyme inactivation, ROS-mediated oxidative stress, DNA damage, and protein synthesis inhibition result in microbial cell death (Pragati et al., 2023). Overall results revealed that biogenic synthesized PSEF2-AgNPs are an effective antibacterial agent for bacterial infection control.

Journal of Chemical Health Risks
www.jchr.org
JCHR (2025) 15(3), 01-07 | ISSN:2251-6727

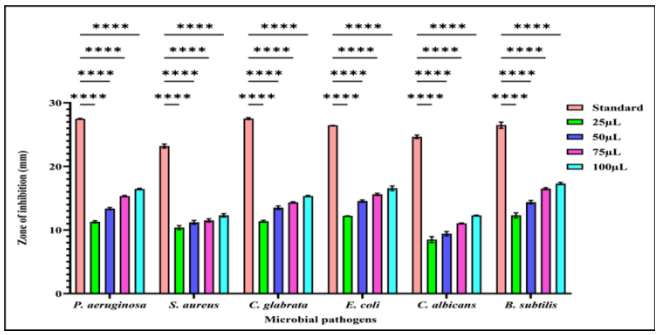

Figure 9. Antimicrobial effect of PSEF2-AgNPs using endophytic fungus *L. pseudotheobromae* PSEF2. Bars represented in mean ± SD (****p < 0.0001, when compared with standard, n=3).

3.5. Antioxidant activity of PSEF2-AgNPs

Ascorbic acid was used as a reference antioxidant to evaluate the synthesized PSEF2-AgNPs capacity to scavenge DPPH. The PSEF2-AgNPs showed inhibition rates of 34.29 ± 0.27%, 45.57 ± 0.19%, 62.06 ± 0.19%, 70.27 ± 0.24%, and 82.71 ± 0.26% at doses of 50, 100, 150, 200, and 250 µg/mL, respectively, with an IC_{50} value of 113.02 µg/mL. The conventional ascorbic acid, by contrast, demonstrated inhibition percentages of 34.29 ± 0.29%, 52.55 ± 0.21%, 64.81 ± 0.22%, 75.82 ± 0.15%, and 88.40 ± 0.27% at the same doses, with an IC_{50} value of 99.89 µg/mL (Figure 10). The dose-dependent scavenging activity suggests that PSEF2-AgNPs effectively neutralize DPPH radicals, although slightly less efficiently than ascorbic acid. The DPPH assay measures the ability of antioxidants to donate hydrogen atoms or electrons to stabilize the free radical DPPH by converting it to DPPH-H (hydrazine form). PSEF2-AgNPs likely contain bioactive molecules from the fungal supernatant that act as electron donors. The antioxidant activity of PSEF2-AgNPs mostly due to the functional groups (e.g., -OH, -NH_2) present on surface of nanoparticles, identified via FTIR, facilitate electron transfer to DPPH (Siddartha et al., 2022; Kubavat et al., 2022).

The H_2O_2 scavenging activity was evaluated and according to the results, PSEF2-AgNPs exhibited a substantial IC_{50} value of 133.34 µg/mL and rates of inhibition of 25.07 ± 0.27%, 41.37 ± 0.19%, 54.71 ± 0.28%, 71.06 ± 0.33%, and 81.49 ± 0.30% at concentrations of 50, 100, 150, 200, and 250 µg/mL, respectively. However, at the same concentrations, ascorbic acid showed inhibition percentages of 32.76 ± 0.13%, 45.96 ± 0.27%, 60.81 ± 0.25%, 72.61 ± 0.19%, and 87.87 ± 0.24%, with an IC_{50} value of 113.44 µg/mL (Figure 10B). H_2O_2 is a ROS that can oxidize cellular components. Antioxidants decompose H_2O_2 into water and oxygen via electron transfer. PSEF2-AgNPs may catalyze H_2O_2 decomposition through direct electron transfer from surface-bound biomolecules. This results in their significant H_2O_2 scavenging activity (Natasha et al., 2018). Similarly, Gupta et al. (2022) reported that Po-AgNPs may scavenge free radicals at lower concentrations. The antioxidant activity of *Penicillium oxalicum* mediated AgNPs was comparable to that of ascorbic acid. Antioxidants protect cells from ROS like hydroxyl radicals, peroxy radicals, peroxynitrite, superoxide, and singlet oxygen. The work coincides with the report of Netala et al, (2016), where biosynthesized AgNPs from *Pestalotiopsis microspora* showed maximum radical scavenging activity of 55.84±1.31% at 100 µg/mL concentrations. H_2O_2 assay revealed highest scavenging activity of 51.14%±1.78% at of 100 µg/mL concentration.

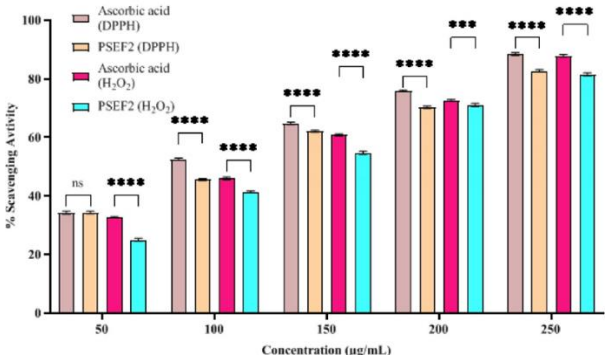

Figure 10. Antioxidant activity of PSEF2-AgNPs at varying concentrations (50–250 µg/mL). (A) DPPH radical scavenging activity and (B) H_2O_2 scavenging activity. Data are presented as mean ± SD ($^{ns}p > 0.1234$, ****p < 0.0002, ****p < 0.0001, when compared with standard, n=3).

3.6. Anticancer activity of PSEF2-AgNPs

The study investigated the anticancer potential of PSEF2-AgNPs biosynthesized from the endophytic fungus *L. pseudotheobromae* against two human cancer cell lines: colorectal adenocarcinoma (Caco2) and hepatocellular carcinoma (HepG2). Using the MTT

Journal of Chemical Health Risks
www.jchr.org
JCHR (2025) 15(3), 01-07 | ISSN:2251-6727

assay, cell viability was evaluated after 24 h exposure to varying concentrations of PSEF2-AgNPs (12.5-200 µg/mL). The results demonstrated a clear dose-dependent cytotoxic effect in both cell lines. For Caco2 cells, progressively decreased cell viability were 87.32%, 83.74%, 74.50%, 49.11% and 2.13% (Figure 11A). Similarly, HepG2 cells showed reduced viability percentages: 80.17%, 73.30%, 70.18%, 48.32% and 12.35% across the same concentration range (Figure 11B). The IC_{50} were determined to be 97.74 µg/mL for Caco2 and 96.54 µg/mL for HepG2 cells, indicating comparable sensitivity to the nanoparticles. When compared to the positive control doxorubicin (4 µM), which showed 21.11% viability in Caco2 and 37.71% in HepG2 cells. The PSEF2-AgNPs exhibited slightly less potency but demonstrated significant anticancer activity, particularly at higher concentrations. These results collectively suggest that PSEF2-AgNPs possess substantial anticancer properties against both colorectal and liver cancer cell lines.

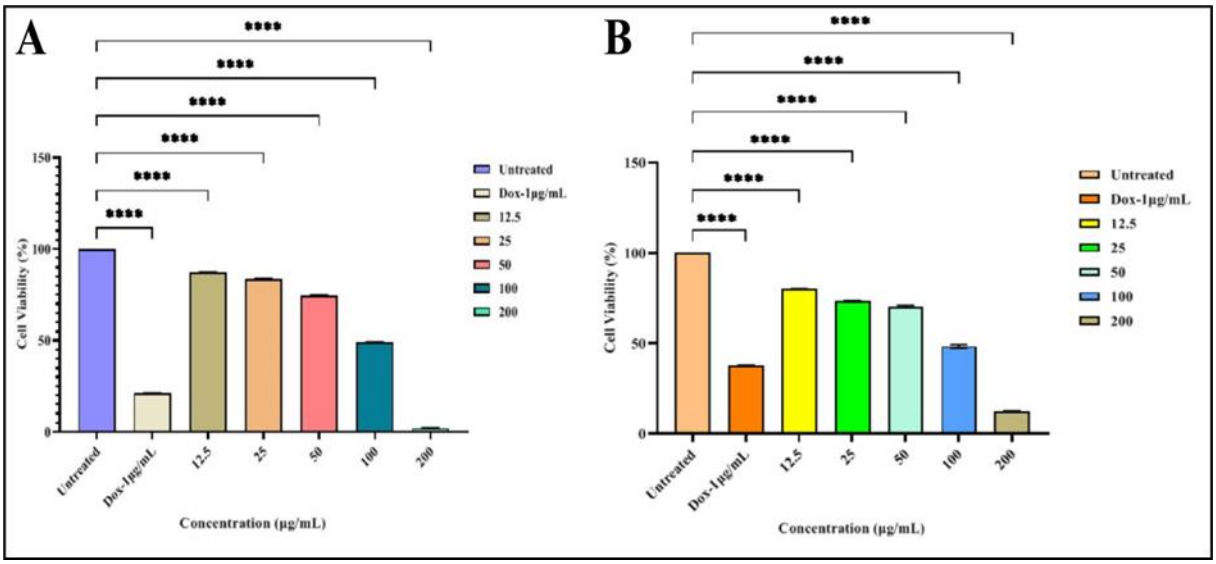

Figure 11. Anticancer activity of PSEF2-AgNPs at varying concentrations (12.5–200 µg/mL) illustrating the dose-dependent reduction in cell viability. (A) Caco2 cell line and (B) HepG2 cell line. Bars represented in mean ± SD (****p < 0.0001, when compared with untreated, n=3).

3.7. Annexin V/Propidium iodide apoptosis detection assay

In order to compare, the study of apoptosis was evaluated using an Annexin V/PI staining test, which was predicated on PSEF2-AgNPs' respective IC_{50} value against the Caco2 and HepG2 cell lines using flow cytometry analysis. The Annexin V/PI apoptosis assay demonstrated that PSEF2-AgNPs significantly reduced cell viability and induced apoptosis in both Caco2 and HepG2 cell lines at their IC_{50} concentrations (97.74 µg/mL and 96.54 µg/mL, respectively). In Caco2 cells, treatment resulted in 38.25% early apoptosis, 35.37% late apoptosis, with only 22.38% viable cells remaining and minimal necrosis (4.0%) (Figure 12). For HepG2 cells (Figure 13), the assay showed 15.31% early apoptosis, 46.35% late apoptosis, 28.71% viable cells, and 9.63% necrosis. Compared to this, doxorubicin control showed 61.28% apoptosis in Caco2 and 45.37% in HepG2. The biosynthesized PSEF2-AgNPs exhibited potent apoptotic effects while maintaining low necrotic activity. These findings confirm the dose-dependent anticancer potential of PSEF2-AgNPs, with Caco2 cells showing greater sensitivity to early apoptotic induction than HepG2 cells. The substantial reduction in viable cell populations (22.38% for Caco2 and 28.71% for HepG2) further supports their therapeutic potential against these cancer cell lines. Annexin-V FITC staining, combined with PI, is a widely used method to distinguish between viable, apoptotic, and necrotic cells. Annexin-V binds specifically to phosphatidylserine, a phospholipid that becomes

Journal of Chemical Health Risks
www.jchr.org
JCHR (2025) 15(3), 01-07 | ISSN:2251-6727

exposed on the outer leaflet of the plasma membrane during the early stages of apoptosis. In contrast, PI is a DNA-binding dye that penetrates only cells with compromised membranes, such as those in late apoptosis or necrosis. This dual staining approach enables clear identification of different cell states: viable cells show low or no FITC and PI fluorescence; early apoptotic cells exhibit strong FITC fluorescence (due to externalized phosphatidylserine) but low PI fluorescence (intact membranes); late apoptotic cells are positive for both FITC and PI; and necrotic cells display low FITC and high PI fluorescence. Thus, simultaneous Annexin V-FITC and PI staining allows for precise quantification and differentiation of cell death stages in apoptosis assays (Bagchi et al., 2016; Salah et al., 2024). This result is in accordance with previous report of Pasha et al, (2022). The study revealed that biosynthesized AgNPs from *Aspergillus niger* showed viable, apoptotic and necrotic cells in HeLa cell line.

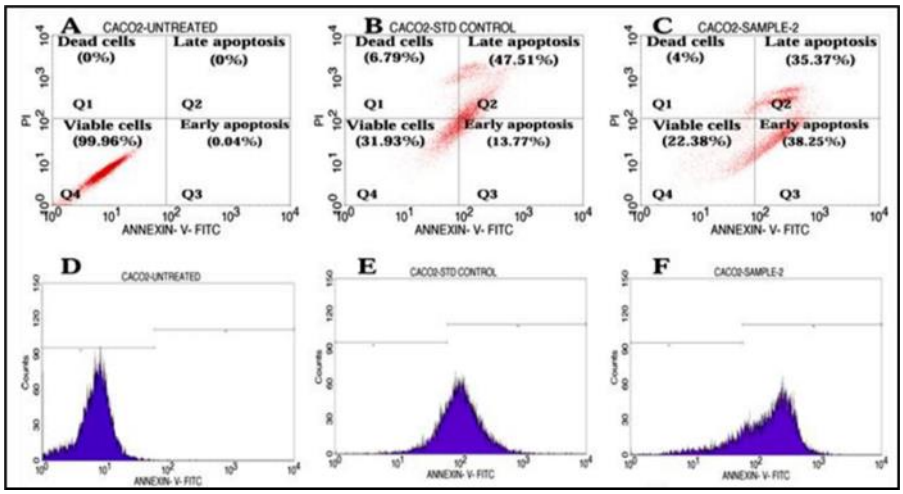

Figure 12. Flow cytometry analysis of Caco2 cells treated with PSEF2-AgNPs at IC_{50} concentration (97.74 µg/mL) using Annexin V-FITC/PI staining.

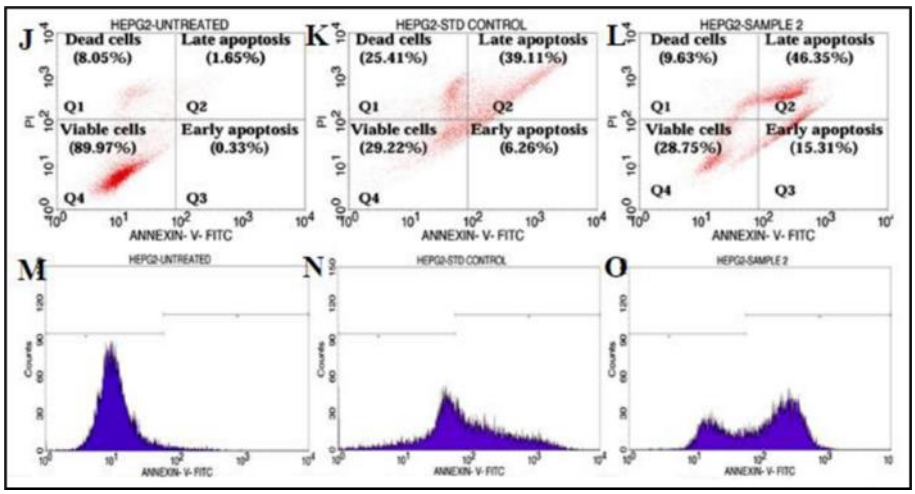

Figure 13. Flow cytometry analysis of HepG2 cells treated with PSEF2-AgNPs at IC_{50} concentration (96.54 µg/mL) using Annexin V-FITC/PI staining.

Journal of Chemical Health Risks
www.jchr.org
JCHR (2025) 15(3), 01-07 | ISSN:2251-6727

3.8. AO/EtBr Fluorescent assay

The AO/EtBr staining assay revealed significant apoptosis and necrosis in Caco2 and HepG2 cells treated with PSEF2-AgNPs at their respective IC_{50} concentrations (97.74 µg/mL and 96.54 µg/mL). Untreated cells exhibited intact green nuclei, indicating viability and a very less number of cells emitting red fluorescence. The PSEF2-AgNPs treated cells showed a significant increase in red fluorescence and a few green fluorescent cells, demonstrating its apoptotic ability. In Caco2 cells, red fluorescence was prominent due to EtBr uptake, suggesting late apoptosis and necrosis (Figure 14A). Similarly, HepG2 cells displayed (Figure 14B) increased red fluorescence, confirming apoptotic and necrotic cell death. The results demonstrated a dose-dependent cytotoxic effect, with PSEF2-AgNPs inducing apoptosis more effectively in Caco2 cells compared to HepG2 cells. Morphological changes such as cell shrinkage, membrane fragmentation, and condensed chromatin were also observed (Netala et al., 2016). The dual staining technique using AO and EtBr is a widely accepted method for evaluating the mechanism of cell death in vitro. AO penetrates all cells, staining the cytoplasm and nucleus and emit green fluorescence, while EtBr only enters cells with compromised membranes, such as apoptotic or necrotic cells, where it binds to minor groove of DNA and emits red fluorescence. In this assay, viable cells fluoresce green due to AO, whereas apoptotic cells take up EtBr, dominating the green signal and appear red. Necrotic cells lack chromatin condensation and typically show orange fluorescence and maintain a nuclear morphology similar to viable cells. This staining approach provides a clear distinction between live, apoptotic, and necrotic cells, making it a reliable tool for assessing cell viability and death pathways in cancer cell lines (Bagchi et al., 2016; Saurabh and Surendra, 2020). Similar findings observed by Krishnaraj et al. (2014) indicated that treatment with the synthesised nanoparticles resulted in an increased number of apoptotic cells in the cancer cell line compared to the control. This study is also related to report of Skóra et al., (2021), where *Saccharomyces cerevisiae* synthesized AgNPs showed where green and red fluorescence indicating live and dead cells due to AO/EtBr staining.

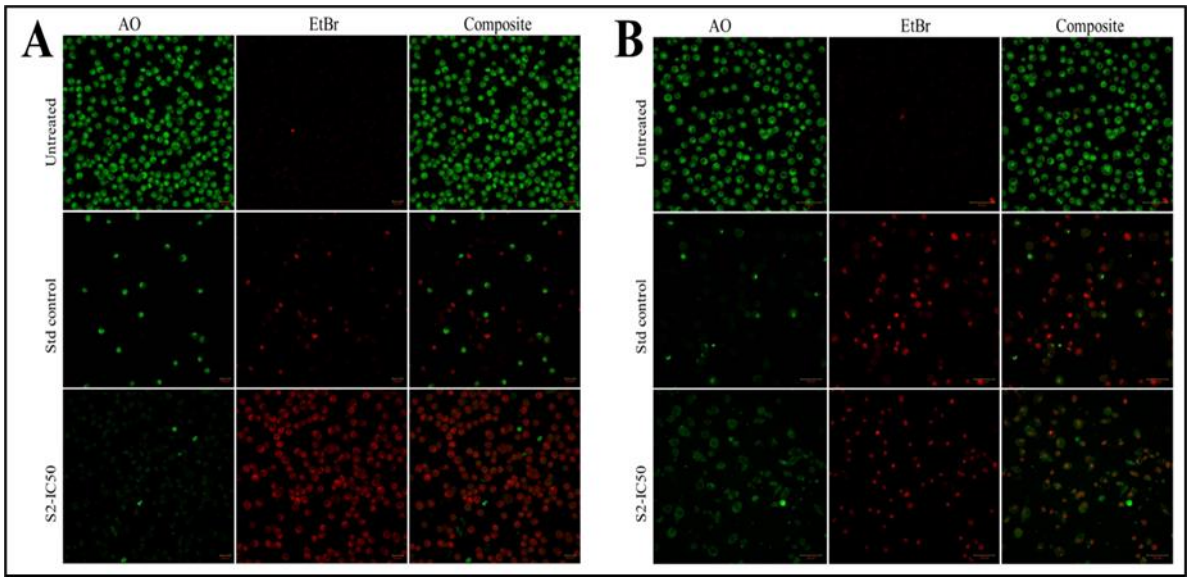

Figure 14. AO/EtBr staining images cancer cell lines treated with IC_{50} concentration of PSEF2- AgNPs. (A) Caco2 cell line and (B) HepG2 cell line.

3.9. ROS assay

ROS are naturally generated in cells as byproducts of metabolic processes like oxidative phosphorylation. Excessive ROS production is closely linked to oxidative stress and the induction of apoptosis, particularly in response to certain anticancer drugs. ROS include highly reactive molecules such as hydroxyl radicals and peroxides with unpaired electrons (Pallavi et al., 2022). The ROS assay demonstrated a

Journal of Chemical Health Risks
www.jchr.org
JCHR (2025) 15(3), 01-07 | ISSN:2251-6727

significant increase in ROS expression in both Caco2 and HepG2 cell lines when treated with PSEF2-AgNPs at their respective IC_{50} concentrations (97.74 µg/mL for Caco2 and 96.54 µg/mL for HepG2). Confocal microscopy revealed intense green fluorescence in treated cells due to the oxidation of H2DCFDA, indicating elevated ROS levels compared to untreated controls. In Caco2 cells, PSEF2-AgNPs induced disassembled cell structures, granular morphology, and brightly stained, condensed nuclei, confirming ROS-mediated DNA damage (Figure 15A). Similarly, HepG2 cells exhibited heightened DCF intensity, along with fragmented nuclei, confirming ROS-mediated cellular damage (Figure 15B). The standard also showed high ROS expression, and nuclear abnormalities, validating the assay. These results suggest that PSEF2-AgNPs trigger apoptosis via oxidative stress, as ROS overproduction disrupts cellular redox balance, leading to DNA damage and organelle dysfunction (Nayaka et al., 2020). Similarly, the Po-AgNPs elicited toxicity by inducing apoptosis in a dose-dependent fashion. The mechanistic action of PoAgNPs involves the induction of ROS, subsequent disruption of intracellular organelles, and ultimately results in apoptosis (Gupta et al., 2022). A similar study showed that an increase in ROS is linked with DNA damage and endorses various apoptotic signalling pathways (Yongxia et al., 2023). These results are also supported by other investigators showing that green synthesized AgNPs exhibit anticancer properties by generating ROS production in various human cancer cell lines, such as liver carcinoma HepG2 (Alyami et al., 2022), breast adenocarcinoma MCF-7 (Erdogan et al., 2019) and cervical cancer cells HeLa (Al-Sheddi et al., 2018).

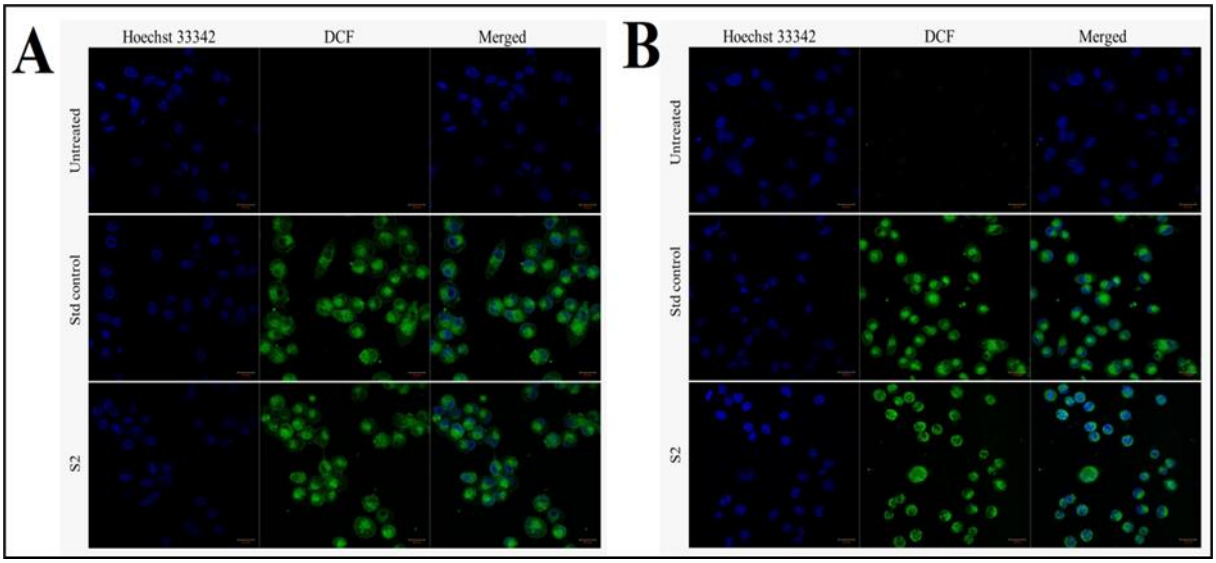

Figure 15. ROS expression of Hoechst and DCF stained images of cancer cells treated IC_{50} concentration of PSEF2-AgNPs. (A) Caco2 cell line and (B) HepG2 cell line.

The anticancer activity of PSEF2-AgNPs against Caco2 and HepG2 cell lines was demonstrated through a series of assays, revealing a dose-dependent cytotoxic effect mediated primarily by apoptosis. Annexin V/PI staining further confirmed the induction of apoptosis, with Caco2 and HepG2 cells. The low necrosis rates suggested a preference for programmed cell death over uncontrolled necrosis. Apoptosis involves apoptotic protein activation, DNA damage, mitochondrial degradation, apoptosome formation, and cell shrinkage (Jain et al., 2021). AgNPs trigger apoptosis via mitochondrial depolarization, DNA damage, ROS generation, cell cycle arrest, and activation of caspase-3 (Kumari et al., 2020). Studies on MCF-7 and T-47D cells show that AgNPs induce ER stress via the unfolded protein response and activate caspases 9 and 7, promoting cell death (Simard et al., 2016). Upregulation of caspases 3, 8, and 9 further accelerates apoptosis (Jain et al., 2021). AgNPs enhance the expression of pro-apoptotic proteins (p53, Bax, and Bid) while downregulating anti-apoptotic proteins (Bcl-2, Bcl-w) (Lee et al., 2011). Green-synthesized AgNPs

Journal of Chemical Health Risks

www.jchr.org

JCHR (2025) 15(3), 01-07 | ISSN:2251-6727

using *Coptis chinensis* increased expression of Bax and Bak while decreasing Bcl-2 and Bcl-XL, modulating mitochondrial apoptosis through ROS generation (Pei et al., 2019; Erdogan et al., 2019). Recent studies highlight the role of AgNPs in elevating oxidative stress and DNA destruction, enhancing apoptosis (Wang et al., 2021). AgNPs also exhibit anti-angiogenic properties by inhibiting VEGF-induced tumour proliferation, preventing the transition from benign to malignant states (Gurunathan et al., 2009; Jain et al., 2021). Overall, the results underscore the potential of PSEF2-AgNPs as an eco-friendly anticancer agent, with apoptosis as the dominant mechanism of action and minimal necrotic effects, making them a promising candidate for further therapeutic development.

4. Conclusion

The present study successfully demonstrated the eco-friendly synthesis of PSEF2-AgNPs using the endophytic fungus *Lasiodiplodia pseudotheobromae* isolated from *Gloriosa superba* L. The biosynthesized PSEF2-AgNPs exhibited remarkable antimicrobial, antioxidant, and anticancer properties. Characterization techniques such as UV-Vis spectroscopy, FTIR, TEM, XRD, and DLS confirmed the formation of spherical, polydisperse AgNPs with an average size of 5-29 nm and high stability. The PSEF2-AgNPs showed significant antimicrobial activity against pathogenic bacteria and yeast, making them promising candidates for developing novel antimicrobial agents. Additionally, the nanoparticles displayed potent antioxidant activity by effectively scavenging DPPH and H_2O_2 radicals. Their potent antioxidant activity suggests possible use in mitigating oxidative stress-related diseases. In vitro cytotoxicity assays revealed dose-dependent anticancer effects against Caco2 and HepG2 cell lines, with IC_{50} values of 97.74 µg/mL and 96.54 µg/mL, respectively. This capacity emphasizes their potential as anticancer therapeutics after through in-vibo studies. Apoptosis induction was confirmed through Annexin V/PI staining, AO/EtBr fluorescence assays, and ROS generation, highlighting PSEF2-AgNPs could be a viable option for targeted cancer therapy. Future research should focus on in vivo studies, which are essential to evaluate the biosafety, pharmacokinetics, and efficacy of PSEF2-AgNPs to ensure their suitability for clinical applications. Exploring the synergistic effects of these nanoparticles with conventional drugs could pave the way for combination therapies to improve treatment outcomes. Further, investigation of the mechanisms underlying the observed biological activities, such as the specific pathways involved in apoptosis and ROS generation, would provide deeper insights into their therapeutic potential.

Acknowledgements:

The authors express gratitude to the Department of Studies in Botany, Karnatak University, Dharwad for granting access to laboratory and instrumentation facilities. The Sophisticated Analytical Instrumentation Facility (SAIF) and University Scientific Instrumentation Centre (USIC) at Karnatak University, Dharwad are acknowledged for providing necessary resources for this study.

Funding: Not applicable.

Ethics Approval: Not applicable.

Data availability: All data generated or analyzed during this study are included in this published manuscript.

Conflicts of Interest: The authors declare no conflict of interest.

References

1. Ahmed, I., Ahmad, N., Mehmood, I., Haq, I. U., Hassan, M., & Khan, M. U. (2016). Applications of nanotechnology in transportation engineering. In A. Khitab & W. Anwar (Eds.), *Advanced research on nanotechnology for civil engineering applications* (pp. 180–207). IGI Global. https://doi.org/10.4018/978-1-5225-0344-6.ch006
2. Ali, E., Abu-Hussien, S. H., Hesham, E., Ahmed, S., Mostafa, H., Gamal, A., & Abd-Elhalim, B. T. (2024). Compatibility and antimicrobial activity of silver nanoparticles synthesized using *Lycopersicon esculentum* peels. *AMB Express*, *14*(1), 120. https://doi.org/10.1186/s13568-024-01774-5
3. Alsareii, S. A., Manaa Alamri, A., AlAsmari, M. Y., Bawahab, M. A., Mahnashi, M. H.,

Journal of Chemical Health Risks

www.jchr.org

JCHR (2025) 15(3), 01-07 | ISSN:2251-6727

Shaikh, I. A., ... Kumbar, V. (2022). Synthesis and characterization of silver nanoparticles from *Rhizophora apiculata* and studies on their wound healing, antioxidant, anti-inflammatory, and cytotoxic activity. *Molecules*, *27*(19), 6306. https://doi.org/10.3390/molecules27196306

4. Al-Sheddi, E. S., Farshori, N. N., Al-Oqail, M. M., Al-Massarani, S. M., Saquib, Q., Wahab, R., ... Siddiqui, M. A. (2018). Anticancer potential of green synthesized silver nanoparticles using extract of *Nepeta deflersiana* against human cervical cancer cells (HeLa). *Bioinorganic Chemistry and Applications*, *2018*(1), 9390784. https://doi.org/10.1155/2018/9390784
5. Alyami, N. M., Alyami, H. M., & Almeer, R. (2022). Using green biosynthesized kaempferol-coated silver nanoparticles to inhibit cancer cells growth: An in vitro study using hepatocellular carcinoma (HepG2). *Cancer Nanotechnology*, *13*(1), 26. https://doi.org/10.1186/s12645-022-00132-z
6. Bagchi, B., Banerjee, S., Arpan, K., Pradip, T., Suman, B., Nur, A. H., & Das, S. (2016). Synthesis of eucalyptus/tea tree oil absorbed biphasic calcium phosphate–PVDF polymer nanocomposite films: A surface active antimicrobial system for biomedical application. *Physical Chemistry Chemical Physics*, *18*, 16775–16785. https://doi.org/10.1039/C6CP03493D
7. Barik, T. K., Mandal, S. M., Mitra, S., Maity, G. C., Roymahapatra, G., & Santra, T. S. (2020). Prospect of nanotechnology: A brief review. *Journal of the Indian Chemical Society*, *97*(11b), 2372–2384. https://doi.org/10.5281/zenodo.5656118
8. Bhattacharya, R., & Mukherjee, P. (2008). Biological properties of "naked" metal nanoparticles. *Advanced Drug Delivery Reviews*, *60*(11), 1289-1306. https://doi.org/10.1016/j.addr.2008.03.013
9. Birla, S. S., Gaikwad, S. C., Gade, A. K., & Rai, M. K. (2013). Rapid synthesis of silver nanoparticles from *Fusarium oxysporum* by optimizing physicocultural conditions. *The Scientific World Journal*, *2013*, 796018. https://doi.org/10.1155/2013/796018
10. Burdușel, A. C., Gherasim, O., Grumezescu, A. M., Mogoantă, L., Ficai, A., & Andronescu, E. (2018). Biomedical applications of silver nanoparticles: An up-to-date overview. *Nanomaterials*, *8*(9), 681. https://doi.org/10.3390/nano8090681
11. Chakraborty, B., Raju, S. K., Abdulrahman, I. A., Kotresha, D., Muthuraj, R., Pallavi, S. S., et al. (2021). Evaluation of antioxidant, antimicrobial and antiproliferative activity of silver nanoparticles derived from *Galphimia glauca* leaf extract. *Journal of King Saud University – Science*, *33*(8), 101660. https://doi.org/10.1016/j.jksus.2021.101660
12. Chen, J., Zhu, Z., Fu, Y., Cheng, J., Xie, J., & Lin, Y. (2021). Identification of *Lasiodiplodia pseudotheobromae* causing fruit rot of citrus in China. *Plants*, *10*(2), 202. https://doi.org/10.3390/plants10020202
13. Clarance, P., Luvankar, B., Sales, J., Khusro, A., Agastian, P., Tack, J. C., & Kim, H. J. (2020). Green synthesis and characterization of gold nanoparticles using endophytic fungi *Fusarium solani* and its in-vitro anticancer and biomedical applications. *Saudi Journal of Biological Sciences*, *27*(2), 706-712. https://doi.org/10.1016/j.sjbs.2019.12.026
14. Das, B., Dash, S. K., Mandal, D., Ghosh, T., Chattopadhyay, S., Tripathy, S., & Roy, S. (2017). Green synthesized silver nanoparticles destroy multidrug resistant bacteria via reactive oxygen species mediated membrane damage. *Arabian Journal of Chemistry*, *10*(6), 862-876. https://doi.org/10.1016/j.arabjc.2015.08.008
15. de Silva, N. I., Phillips, A. J. L., Liu, J. K., Lumyong, S., & Hyde, K. D. (2019). Phylogeny and morphology of *Lasiodiplodia* species associated with Magnolia forest plants. *Scientific Reports*, *9*, 14355. https://doi.org/10.1038/s41598-019-50804-x
16. Devi, L. S., & Joshi, S. R. (2015). Ultrastructures of silver nanoparticles biosynthesized using endophytic fungi. *Journal of Microscopy and Ultrastructure*,

Journal of Chemical Health Risks

www.jchr.org

JCHR (2025) 15(3), 01-07 | ISSN:2251-6727

3(1), 29-37. https://doi.org/10.1016/j.jmau.2014.10.004

17. Ekaterina, O. M. (2020). Silver nanoparticles: Mechanism of action and probable bio-application. *Journal of Functional Biomaterials*, *11*(4), 84. https://doi.org/10.3390/jfb11040084
18. Elvira, I. M. R., Alfredo, R. V. N., Karla, J. M., Luis, E. G. M., Katrin, Q., & Ernestina, C. L. (2022). Optimized synthesis of small and stable silver nanoparticles using intracellular and extracellular components of fungi: An alternative for bacterial inhibition. *Antibiotics*, *11*(6), 800. https://doi.org/10.3390/antibiotics11060800
19. El-Zawawy, N. A., Ali, S. S., & Nouh, H. S. (2023). Exploring the potential of *Rhizopus oryzae* AUMC14899 as a novel endophytic fungus for the production of L-tyrosine and its biomedical applications. *Microbial Cell Factories*, *22*(1), 31. https://doi.org/10.1186/s12934-023-02041-1
20. Enerelt, U., Bum-Erdene, B., Aminaa, G., Nominchimeg, S., & Tsogbadrakh, M. (2021). Antibacterial activity and characteristics of silver nanoparticles biosynthesized from *Carduus crispus*. *Scientific Reports*, *11*, 21047. https://doi.org/10.1038/s41598-021-00520-2
21. Erdogan, O., Abbak, M., Demirbolat, G. M., Birtekocak, F., Aksel, M., Pasa, S., & Cevik, O. (2019). Green synthesis of silver nanoparticles via *Cynara scolymus* leaf extracts: The characterization, anticancer potential with photodynamic therapy in MCF7 cells. *PLoS ONE, 14*(6), e0216496. https://doi.org/10.1371/journal.pone.0216496
22. Guilger-Casagrande, M., & Lima, R. D. (2019). Synthesis of silver nanoparticles mediated by fungi: A review. *Frontiers in Bioengineering and Biotechnology, 7*, 287. https://doi.org/10.3389/fbioe.2019.00287
23. Gupta, P., Rai, N., Verma, A., Saikia, D., Singh, S. P., Kumar, R., & Gautam, V. (2022). Green-based approach to synthesize silver nanoparticles using the fungal endophyte *Penicillium oxalicum* and their antimicrobial, antioxidant, and in vitro anticancer potential. *ACS Omega, 7*(50), 46653-46673. https://doi.org/10.1021/acsomega.2c05605
24. Gurunathan, S., Lee, K. J., Kalishwaralal, K., Sheikpranbabu, S., Vaidyanathan, R., & Eom, S. H. (2009). Antiangiogenic properties of silver nanoparticles. *Biomaterials, 30*(31), 6341-6350. https://doi.org/10.1016/j.biomaterials.2009.08.008
25. Hikmet, R. A., & Hussein, N. N. (2021). Mycosynthesis of silver nanoparticles by *Candida albicans* yeast and its biological applications. *Archives of Razi Institute, 76*(4), 857. https://doi.org/10.22092/ari.2021.355935.1741
26. Hu, X., Saravanakumar, K., Jin, T., & Wang, M. H. (2019). Mycosynthesis, characterization, anticancer and antibacterial activity of silver nanoparticles from endophytic fungus *Talaromyces purpureogenus*. *International Journal of Nanomedicine, 14*, 3427-3438. https://doi.org/10.2147/IJN.S200817
27. Huzefa, A. R., Miller, A. N., Pearce, C. J., & Oberlies, N. H. (2017). Fungal identification using molecular tools: A primer for the natural products research community. *Journal of Natural Products, 80*(3), 756-770. https://doi.org/10.1021/acs.jnatprod.6b01085
28. Iuliana, R., Mariana, C., Raluca, Ș. B., Cristina, F., Elvira, A., Ioana, C. G., Mihaela, D., Zamfir, L. G., Gurban, A. M., & Luiza, J. (2024). Extracellular biosynthesis, characterization and antimicrobial activity of silver nanoparticles synthesized by filamentous fungi. *Journal of Fungi, 10*(11), 798. https://doi.org/10.3390/jof10110798
29. Jain, N., Jain, P., Rajput, D., & Patil, U. K. (2021). Green synthesized plant-based silver nanoparticles: Therapeutic prospective for anticancer and antiviral activity. *Micro and Nano Systems Letters, 9*, 5. https://doi.org/10.1186/s40486-021-00131-6
30. Janakiraman, V., Govindarajan, K., & CR, M. (2019). Biosynthesis of silver nanoparticles from endophytic fungi, and its cytotoxic activity. *BioNanoScience, 9*, 573-579. https://doi.org/10.1007/s12668-019-00631-1

31. Jerónimo, O. E., Juliana, O. E., Claudia, P. O. O., & Natalia, A. G. V. (2021). Synthesis of silver nanoparticles using white-rot fungus Anamorphous *Bjerkandera* sp. R1: Influence of silver nitrate concentration and fungus growth time. *Scientific Reports, 11*, 3842. https://doi.org/10.1038/s41598-021-82514-8
32. Joshi, B. C., Durgapal, S., Mukhija, M., & Anurag, B. (2024). An overview on the phytopharmacological insights into *Gloriosa superba* L. (Kalahari): A promising endangered plant species. *Discover Plants, 1*, 57. https://doi.org/10.1007/s44372-024-00054-7
33. Juan, W., Samuel, K. O., Shu, W., Wang, J., Lei, X., Yinan, R., & Hu, Y. (2022). Endophytic fungi: An effective alternative source of plant-derived bioactive compounds for pharmacological studies. *Journal of Fungi, 8*(2), 205. https://doi.org/10.3390/jof8020205
34. Kavithamani, D., Umadevi, M., & Geetha, S. (2013). A review on *Gloriosa superba* L. as a medicinal plant. *Indian Journal of Research in Pharmacy and Biotechnology, 1*(4), 554-557.
35. Khan, Y., Sadia, H., Ali S. S. Z., Khan, M. N., Shah, A. A., Ullah, N., & Khan, M. I. (2022). Classification, synthetic, and characterization approaches to nanoparticles, and their applications in various fields of nanotechnology: A review. *Catalysts, 12*(11), 1386. https://doi.org/10.3390/catal12111386
36. Krishnaraj, C., Muthukumaran, P., Ramachandran, R., Balakumaran, M. D., & Kalaichelvan, P. T. (2014). *Acalypha indica* Linn: Biogenic synthesis of silver and gold nanoparticles and their cytotoxic effects against MDA-MB-231, human breast cancer cells. *Biotechnology Reports (Amst), 4*, 42-49. https://doi.org/10.1016/j.btre.2014.08.002
37. Kubavat, K., Trivedi, P., Ansari, H., Kongor, A., Panchal, M., Jain, V., & Sindhav, G. (2022). Green synthesis of silver nanoparticles using dietary antioxidant rutin and its biological contour. *Beni-Suef University Journal of Basic and Applied Sciences, 11*, 115. https://doi.org/10.1186/s43088-022-00297-x
38. Kumari, R., Saini, A. K., Kumar, A., & Saini, R. V. (2020). Apoptosis induction in lung and prostate cancer cells through silver nanoparticles synthesized from *Pinus roxburghii* bioactive fraction. *Journal of Biological Inorganic Chemistry, 25*(1), 23-37. https://doi.org/10.1007/s00775-019-01729-3
39. Lee, Y. S., Kim, D. W., Lee, Y. H., Oh, J. H., Yoon, S., Choi, M. S., Lee, S. K., Kim, J. W., Lee, K., & Song, C. W. (2011). Silver nanoparticles induce apoptosis and G2/M arrest via PKCζ-dependent signaling in A549 lung cells. *Archives of Toxicology, 85*(12), 1529-1540. https://doi.org/10.1007/s00204-011-0714-1
40. Liaqat, N., Jahan, N., Anwar, T., & Qureshi, H. (2022). Green synthesized silver nanoparticles: Optimization, characterization, antimicrobial activity, and cytotoxicity study by hemolysis assay. *Frontiers in Chemistry, 10*, 952006. https://doi.org/10.3389/fchem.2022.952006
41. Math, H. H., Shashiraj, K. N., Kumar, R. S., Rudrappa, M., Bhat, M. P., Basavarajappa, D. S., & Nayaka, S. (2023). Investigation of in vitro anticancer and apoptotic potential of biofabricated silver nanoparticles from *Cardamine hirsuta* (L.) leaf extract against Caco-2 cell line. *Inorganics, 11*(8), 322. https://doi.org/10.3390/inorganics11080322
42. Natasha, A., Shah, M., Saleem, S., & Rahman, H. (2018). Plant-mediated synthesis of silver nanoparticles and their biological applications. *Bulletin of the Chemical Society of Ethiopia, 32*(3), 469-479. https://doi.org/10.4314/bcse.v32i3.6
43. Nayaka, S., Chakraborty, B., Bhat, M. P., Nagaraja, S. K., Airodagi, D., Swamy, P. S., & Kanakannanavar, B. (2020). Biosynthesis, characterization, and in vitro assessment on cytotoxicity of actinomycete-synthesized silver nanoparticles on *Allium cepa* root tip cells. *Beni-Suef University Journal of Basic and Applied Sciences, 9*, 1-18. https://doi.org/10.1186/s43088-020-00074-8
44. Netala, V. R., Murali, S. B., Bobbu, P., Vijaya, B. B., Sani, A., Rao, V. J., & Vijaya, T. (2016). Biogenesis of silver nanoparticles

using endophytic fungus *Pestalotiopsis microspora* and evaluation of their antioxidant and anticancer activities. *International Journal of Nanomedicine, 11*, 5683-5696. https://doi.org/10.2147/IJN.S112857

45. Pallavi, S. S., Hassan, A. R., Asmatanzeem, B., Shaik, K. N., & Sreenivasa, N. (2022). Green synthesis of silver nanoparticles using *Streptomyces hirsutus* strain SNPGA-8 and their characterization, antimicrobial activity, and anticancer activity against human lung carcinoma cell line A549. *Saudi Journal of Biological Sciences, 29*(1), 228-238. https://doi.org/10.1016/j.sjbs.2021.08.084
46. Pasha, A., Kumbhakar, D. V., Sana, S. S., Ravinder, D., Lakshmi, B. V., Kalangi, S. K., & Pawar, S. C. (2022). Role of biosynthesized Ag-NPs using *Aspergillus niger* (MK503444.1) in antimicrobial, anti-cancer and anti-angiogenic activities. *Frontiers in Pharmacology, 12*, 812474. https://doi.org/10.3389/fphar.2021.812474
47. Pei, J., Fu, B., Jiang, L., & Sun, T. (2019). Biosynthesis, characterization, and anticancer effect of plant-mediated silver nanoparticles using *Coptis chinensis*. *International Journal of Nanomedicine, 14*, 1969-1978.
48. Pragati, R. M., Santosh, P., Anna, D. F., Gianluigi, F., Ivan, M., & Galdiero, M. (2023). Silver nanoparticles: Bactericidal and mechanistic approach against drug-resistant pathogens. *Microorganisms, 11*(2), 369. https://doi.org/10.3390/microorganisms11020369
49. Rudrappa, M., Kumar, R. S., Basavarajappa, D. S., Bhat, M. P., Nagaraja, S. K., Almansour, A. I., & Nayaka, S. (2023). *Penicillium citrinum* NP4 mediated production, extraction, physicochemical characterization of the melanin, and its anticancer, apoptotic, photoprotection properties. *International Journal of Biological Macromolecules, 245*, 125547. https://doi.org/10.1016/j.ijbiomac.2023.125547
50. Saba, M., Farooq, S., Alessa, A. H., et al. (2025). Green synthesis of silver nanoparticles using keratinase from *Pseudomonas aeruginosa*-C1M, characterization and applications as novel multifunctional biocatalyst. *BMC Biotechnology, 25*, 27. https://doi.org/10.1186/s12896-025-00959-5
51. Safi, U. R. Q., & Jam, N. A. (2021). Nanoparticles: Mechanism of biosynthesis using plant extracts, bacteria, fungi, and their applications. *Journal of Molecular Liquids, 334*, 116040. https://doi.org/10.1016/j.molliq.2021.116040
52. Salah, A. A., Hassan, A. A., Abdullah, M. A., & Zamri, C. (2024). Flow cytometry-based quantitative analysis of cellular protein expression in apoptosis subpopulations: A protocol. *Heliyon, 10*(13), e33665. https://doi.org/10.1016/j.heliyon.2024.e33665
53. Sandhu, S. S., Shukla, H., & Shukla, S. (2017). Biosynthesis of silver nanoparticles by endophytic fungi: Its mechanism, characterization techniques and antimicrobial potential. *African Journal of Biotechnology, 16*(14), 683-698. https://doi.org/10.5897/AJB2017.15873
54. Saranya, C. R., Paul, B. F., & Sarkar, D. (2021). Hepatocellular carcinoma (HCC): Epidemiology, etiology and molecular classification. *Advances in Cancer Research, 149*, 1-61. https://doi.org/10.1016/bs.acr.2020.10.001
55. Saurabh, Y., & Surendra, K. T. (2020). Cytotoxicity and induction of apoptosis in melanoma (MDA-MB-435S) cells by emodin. *Journal of Scientific Research, 64*(2), 158-165. https://doi.org/10.37398/JSR.2020.640223
56. Seetharaman, P. K., Chandrasekaran, R., Gnanasekar, S., Chandrakasan, G., Gupta, M., Manikandan, D. B., & Sivaperumal, S. (2018). Antimicrobial and larvicidal activity of eco-friendly silver nanoparticles synthesized from endophytic fungi *Phomopsis liquidambaris*. *Biocatalysis and Agricultural Biotechnology, 16*, 22-30. https://doi.org/10.1016/j.bcab.2018.07.006
57. Seetharaman, P. K., Chandrasekaran, R., Periakaruppan, R., Gnanasekar, S., Sivaperumal, S., Abd-Elsalam, K. A., & Kuca, K. (2021). Functional attributes of myco-synthesized silver nanoparticles from endophytic fungi: A new implication in

biomedical applications. *Biology, 10*(6), 473. https://doi.org/10.3390/biology10060473

58. Sergei, A. K., Olga, V. A., Alexander, E. V., Vladimir, N. U., Guy, W. D., Margarita, A. B., Valery, A. P., & Elena, N. T. (2021). Isolation and characterization of human colon adenocarcinoma stem-like cells based on the endogenous expression of the stem markers. *International Journal of Molecular Sciences, 22*(9), 4682. https://doi.org/10.3390/ijms22094682
59. Sharma, A., Sagar, A., Rana, J., & Rani, R. (2022). Green synthesis of silver nanoparticles and its antibacterial activity using fungus *Talaromyces purpureogenus* isolated from *Taxus baccata* Linn. *Micro and Nano Systems Letters, 10*, 2. https://doi.org/10.1186/s40486-022-00144-9
60. Shobha, M., Sampath Kumara, K. K., & Prakash, H. S. (2019). Fungal endophytes associated with *Gloriosa superba* (L.). *Proceedings of the National Academy of Sciences, India Section B: Biological Sciences, 89*, 1335-1342. https://doi.org/10.1007/s40011-018-1053-2
61. Siddartha, B., Riya, M., Anjali, P., Arpana, V., Archana, G., Pati, P. R., & Chang, C. M. (2022). Determination of antioxidants by DPPH radical scavenging activity and quantitative phytochemical analysis of *Ficus religiosa*. *Molecules, 27*(4), 1326. https://doi.org/10.3390/molecules27041326
62. Simard, J. C., Durocher, I., & Girard, D. (2016). Silver nanoparticles induce irremediable endoplasmic reticulum stress leading to unfolded protein response dependent apoptosis in breast cancer cells. *Apoptosis, 21*, 1279-1290. https://doi.org/10.1007/s10495-016-1285-7
63. Singh, D., Rathod, V., Ninganagouda, S., Hiremath, J., Singh, A. K., & Mathew, J. (2014). Optimization and characterization of silver nanoparticle by endophytic fungi *Penicillium* sp. isolated from *Curcuma longa* (turmeric) and application studies against MDR *E. coli* and *S. aureus*. *Bioinorganic Chemistry and Applications, 2014*, 408021. https://doi.org/10.1155/2014/408021
64. Skóra, B., Krajewska, U., Nowak, A., Andrzej, D., Adriana, B., & Małgorzata, K. L. (2021). Noncytotoxic silver nanoparticles as a new antimicrobial strategy. *Scientific Reports, 11*, 13451. https://doi.org/10.1038/s41598-021-92812-w
65. Spagnoletti, F. N., Spedalieri, C., Kronberg, F., & Giacometti, R. (2019). Extracellular biosynthesis of bactericidal Ag/AgCl nanoparticles for crop protection using the fungus *Macrophomina phaseolina*. *Journal of Environmental Management, 231*, 457-466. https://doi.org/10.1016/j.jenvman.2018.10.081
66. Toppo, P., Jangir, P., Mehra, N., Rupam, K., & Piyush, M. (2024). Bioprospecting of endophytic fungi from medicinal plant *Anisomeles indica* L. for their diverse role in agricultural and industrial sectors. *Scientific Reports, 14*, 588. https://doi.org/10.1038/s41598-023-51057-5
67. Tyagi, S., Tyagi, P. K., Gola, D., Chauhan, N., & Bharti, R. K. (2019). Extracellular synthesis of silver nanoparticles using entomopathogenic fungus: Characterization and antibacterial potential. *SN Applied Sciences, 1*, 1-9. https://doi.org/10.1007/s42452-019-1593-y
68. Ungár, T. (2004). Microstructural parameters from X-ray diffraction peak broadening. *Scripta Materialia, 51*(8), 777-781. https://doi.org/10.1016/j.scriptamat.2004.05.007
69. Vasudeva, N. R., Kotakadi, V. S., Bobbu, P., Gaddam, S. A., & Tartte, V. (2016). Endophytic fungal isolate mediated biosynthesis of silver nanoparticles and their free radical scavenging activity and anti-microbial studies. *3 Biotech, 6*, 1-9. https://doi.org/10.1007/s13205-016-0433-7
70. Velgosova, O., Dolinská, S., Podolská, H., Mačák, L., & Čižmárová, E. (2024). Impact of plant extract phytochemicals on the synthesis of silver nanoparticles. *Materials, 17*(10), 2252. https://doi.org/10.3390/ma17102252
71. Wang, D., Xue, B., Wang, L., Zhang, Y., Liu, L., & Zhou, Y. (2021). Fungus-mediated green synthesis of nano-silver using *Aspergillus sydowii* and its antifungal/antiproliferative

activities. *Scientific Reports, 11*, 10356. https://doi.org/10.1038/s41598-021-89854-5

72. Xiaoyu, G., & Gregory, V. L. (2018). Progress towards standardized and validated characterizations for measuring physicochemical properties of manufactured nanomaterials relevant to nano health and safety risks. *NanoImpact, 9*, 14-30. https://doi.org/10.1016/j.impact.2017.09.002
73. Yongxia, Z., Ye, X., Zhifeng, X., Awais, I., Irma, A., Marta, M., Bernardo, L. T., & María, R. M. L., et al. (2023). Cancer metabolism: The role of ROS in DNA damage and induction of apoptosis in cancer cells. *Metabolites, 13*(7), 796. https://doi.org/10.3390/metabo13070796